Metamodel for thermal field : application to GTA welding

Zaid Boutaleb, Issam Bendaoud, Sébastien Rouquette, Fabien Soulié

77th IIW Annual Assembly and International Conference on Welding and Joining 7-12 July 2024 Rhodes, Greece

Metamodel for thermal field : application to GTA welding

Z. BOUTALEB, I. BENDAOUD, S. ROUQUETTE, F. SOULIÉ*

LMGC, Univ. Montpellier, CNRS, Montpellier, France

Abstract. The thermal cycles in arc welding are crucial as they determine the metallurgy, residual stresses, and distortions of welded parts. Thermal simulations are often used as a preliminary stage, with two main methods: either a multiphysics approach or an equivalent heat source approach. The latter is used to reduce computation times. This study aims at predicting the thermal field using a metamodel approach and experimental data. A non-intrusive, contactless sensor is used for monitoring the weld pool contour. This contour is defined as the reference experimental data. A compact camera integrated into the welding setup acquires weld pool images for contour detection during GTAW operation. A numerical design of experiments is conducted by varying heat source parameters in purely conductive thermal finite element analysis. The resulting dataset is used for machine learning training. An optimization approach employs a polynomial regression model to estimate the heat source from the weld pool contour, while algorithms like K-Nearest Neighbors (K-NN) predict the thermal field from estimated heat source. By employing this data-driven approach, we expect a significant reduction in computational time to obtain the thermal field from the melt pool contour.

Keywords: Weld Pool, Contour Detection, Heat flux modelling, Surrogate Model, Machine learning

1 Introduction

Arc welding is a widely used technique for joining metallic materials. An electric arc is created between an electrode, fusible or not, and the metallic parts to join in order to produce a local melting of the parts edges in contact. The heat generated from the arc is transferred to the parts through their surfaces. A melt pool forms when the metal reaches its melting point. The melted metal pool is shielded against oxidation with an inert gas or mixture of inert and active gas. Fluid movements develop within the weld pool and redistribute the heat everywhere in the pool. The weld pool growth until the heat balance is achieved. Once the welding torch moves away, the melted metal solidifies what ensures the material continuity. The welding process under investigation is the Gas Tungsten Arc Welding (GTAW) which is widely used for joining metallic parts. GTAW process is commonly used in industries such as power plants, petrochemicals, food-processing ...

Critical defects such as cracking can occur, primarily due to stresses that develop from the welding thermal cycle. Structural defects that arise during welding require a focused research effort on improving structural integrity. Structural integrity of welded assemblies relies mainly on the final micro-structures in the heat affected and melted zones and the residual stresses [1,2].

Thermal is central in fusion welding process as the thermal history determines the final stress and metallurgical states of the finished part. Thermal fields can be obtained using multiphysics [3] or equivalent heat source approaches [4]. The latter simplifies the process by focusing on thermal diffusion phenomena, requiring estimation of heat source parameters.

Like most engineering processes, the arc welding process depends on various operating parameters, including voltage, current, travelling speed, and other less critical parameters such as gas composition and flow, contact tip distance, and torch angle. Studying or optimizing these parameters through numerical simulations requires substantial computational resources and time [5,6]. For each set of operating parameters, numerical simulations need the estimation of unknown parameters, which requires multiple parametric simulations to converge to experimental data observations. Optimizing these parameters to enhance reliability using numerical methods involves formulating a cost function or a functional from the numerical representation of the process physical reality. This optimization demands multiple numerical evaluations before achieving a specific criterion. Given the large number of numerical evaluations, using classical models like finite element analysis would result in impractically long computational times. Therefore, surrogate modeling is a valuable technique. Surrogate modeling involves creating a mathematical model for which previous numerical simulations serve as the training dataset. Once the training step is completed, the data-driven surrogate can predict quantities of interest much faster [7].

In this work, we present a methodology using image sensing and signals information about operating parameters (current and voltage) to predict the thermal field. The methodology involves solving an inverse problem as a preliminary step for modeling parameter estimation; then, given these estimated parameters, the thermal field is predicted.

2 Method

2.1 Experimental setup and data acquisition

Experimental set-up of TIG welding has been designed to monitor the welding pool shape morphology, to observe fluid flow at its surface, and possibly solidification mechanism. The setup includes a welding generator, 316L stainless alloy 1.5mm sheet, clamping support mounted on slides and camera equipment as illustrated in figure 1. The weld is performed using a static TIG welding generator with a tungsten electrode of 2.4mm diameter and sharpened with 30° angle. A 316L sheet of size 150x70x1.5mm^3 is clamped on a mobile support mounted on slides. The motion of the support is driven by motors, which are regulated with an Arduino UNO board to ensure accurate translation. A camera is positioned to monitor the weld pool's bottom surface.

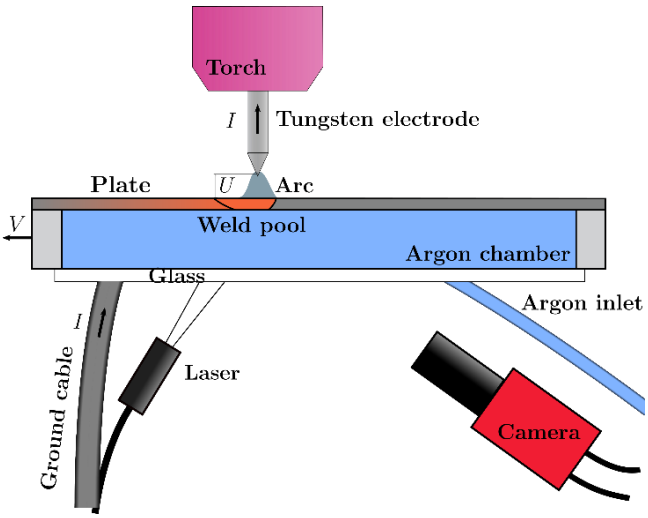

Fig. 1. Schematic representation of the experimental setup (fig. from [8]-modified).

During the welding operation, a shielding gas is emitted from the TIG torch to protect the weld pool from oxidation at the top surface. Welding process parameters are monitored by measuring the current I and the arc voltage U.

Arc voltage and current are almost constant, their respective averaged values are given by 8.58V and 81.7A. Energy delivered by the generator within time is calculated as the product of the arc voltage and current which correspond to 700.9W. Welding speed during experiment was maintained constant at 2.3mm/s.

As the electric arc generates heat, a portion of that heat is absorbed at the top surface of the plate. As the heat absorbed accumulates in the local region, metal reaches its melting point which implies that weld pool appears. The thickness of the plate favorizes the full penetration of the weld pool, allowing the observation of the molten pool from underneath surface. To ensure clarity of the molten pool's fluid surface, argon chamber enclosure purges oxygen to prevent oxidation. The laser is pointed towards the melt pool underneath surface to illuminate that region.

The camera is pointed towards underneath surface to monitor the molten pool dimensions. With laser illumination, the contrast between the solid region and the molten region is easy to distinguish. The frontier separating the solid and liquid phases of the metal determines the dimension of the molten pool. To automate the procedure of molten pool contour identifications, algorithms have been developed in precedent studies. Initially, a Template Matching filter is applied to enhance the grey levels of the targeted pixels. This is followed by a Canny filter, designed for edge detection by tracing lines following the gradient of light intensity. Lastly, the Alpha Shapes algorithm is used to delineate the probable contour of the weld pool [8].

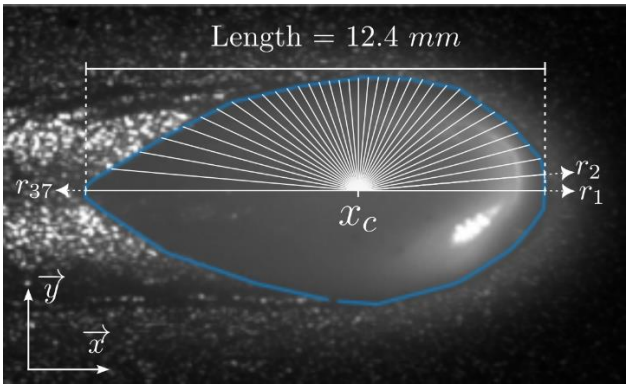

Fig. 2. Weld pool imaging results, contour identification and centroid-rays description.

A contour in an image represents a set of pixels arranged in a Cartesian grid. This contour delineates the boundary between solid and liquid metal phases as shown in figure 2. Comparing two distinct contours, whether from experimental data or numerical simulations, presents limitation. Typically, the comparison involves calculating differences; however, the pixel counts describing each contour often vary, which complicates direct comparisons. Currently, no straightforward criteria exist for evaluating these differences. To address this limitation, we propose using a centroid-rays based description. First, we determine the centroid of the weld pool. From this point, we draw rays extending through the contour at various angles. We start at the welding direction and increment the angle by 5 degrees in a counterclockwise direction, continuing until reaching 180 degrees as seen in figure 2. This method allows for a more standardized comparison of contours.

2.2 Thermal modelling

The thermal modelling is limited to half 316L metal sheet as presented in figure 3.

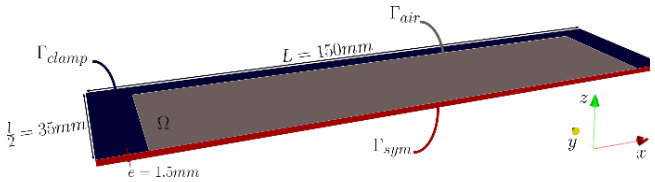

Fig. 3. Geometric modeling domain, boundary conditions.

Thermophysical properties of 316L stainless steel alloy are temperature dependent.

An enthalpic formulation is used to compute the temperature field. The equation of conservation of energy is :

$$\frac{\partial H}{\partial t} - \mathrm{div}(\lambda(T)\nabla T) = 0 \quad \forall (x,y,z) \in \Omega \quad \forall t \in [0, t_f]$$

with enthalpy $H(T) = \int_{T_0}^{T} \rho C_p(u)du$ interpreted as the heat energy of a material at a given temperature, ρ is the mass density, Cp is the specific heat.

Considering the symmetry of the metal sheet, half of the domain is studied. On the symmetry surface Γ_{sym}, adiabatic heat exchange is imposed. On the surfaces regions in contact with air, convective and radiative boundary conditions are imposed. On the clamped surfaces, the thermal contact is modelled similarly to a convective boundary condition with higher convective coefficient comparing with the convective coefficient with air.

The heat input is modeled as a double elliptical equivalent heat source represented in Figure 4. The energy density is distributed into two semi-elliptical regions, following a normal distribution.

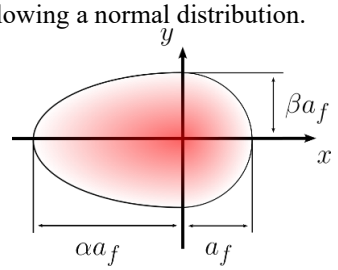

Fig. 4. Equivalent heat source representation with the mathematical description:

$$q_f(x,y,t) = \frac{12\eta UI}{\pi\beta a_f^2(1+\alpha)} e^{-3\left(\left(\frac{(x-Vt)^2}{af}\right)^2 + \left(\frac{y}{\beta a_f}\right)^2\right)} \quad \forall x \geq 0$$

$$q_r(x,y,t) = \frac{12\eta UI}{\pi\beta a_f^2(1+\alpha)} e^{-3\left(\left(\frac{(x-Vt)^2}{\alpha af}\right)^2 + \left(\frac{y}{\beta a_f}\right)^2\right)} \quad \forall x < 0$$

q_f is the front heat source function distribution and q_r the rear function distribution. With η the efficiency taking account of energy loses. This mathematical representation considers the effective heat absorption, where the equivalent heat source is influenced by process parameters such as voltage U, current I, and welding speed V.

Given these modeling considerations, unknown parameters require estimation for good representation of physical reality. The unknown parameters include the efficiency η, geometrical dimensions of the equivalent heat source (af,α, β), and the thermal conductivity multiplier cc within the melted region.

2.3 Thermal field prediction methodology

The global methodology for thermal field reconstruction given welding parameters and knowing observed welding pool is presented in this section. The methodology is derived into two main steps, the first step is the estimation of the unknown heat source parameters, the second step consists in reconstructing the thermal field considering the estimated unknown parameters. The following diagram in figure 5 shows the global methodology.

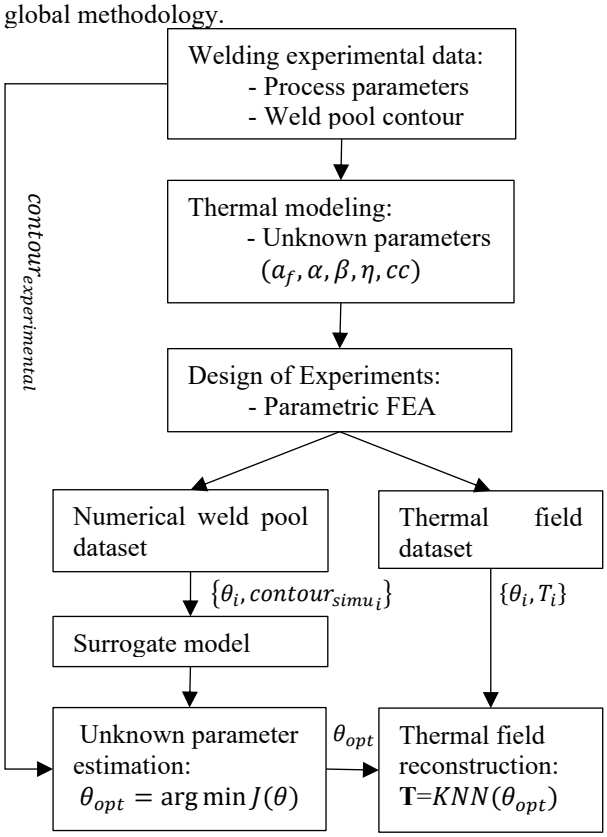

Fig. 5. Diagram methodology. Unknown parameter estimation/thermal field reconstruction

In the previous sections we presented the experimental setup and thermal modeling description. Thermal modeling considers unknown parameters that have to be estimated. A design of experiments is employed to investigate space of unknown modeling parameters. Sobol quasi-random sequence is used to generate a set of 128 sample points, ensuring an uniform distribution across the parameters space. Each sample point represents a unique combination of parameters values. For each of these combinations, a finite element analysis (FEA) simulation is performed.

In one hand, weld pool contours from these simulations are extracted, providing a dataset that links the input parameters to the observed weld pool characteristics. This dataset is used to train a surrogate model, a machine learning model that approximates the relationship between the input parameters and the weld pool morphology. The trained surrogate model is then used

in an optimization algorithm to estimate the unknown parameters. The optimization problem is formulated as finding the set of parameters that minimizes the discrepancy between the predicted weld pool morphology from the surrogate model and the actual weld pool morphology observed in experiments. This is achieved by minimizing a cost function that quantifies this discrepancy. The optimum set of parameters resulting from inverse problem solution is given by:

$$\theta_{opt} = \left[a_f = 2.6mm, \alpha = 4.1, \beta = 2, \eta = 0.8, cc = 1\right] \quad (1)$$

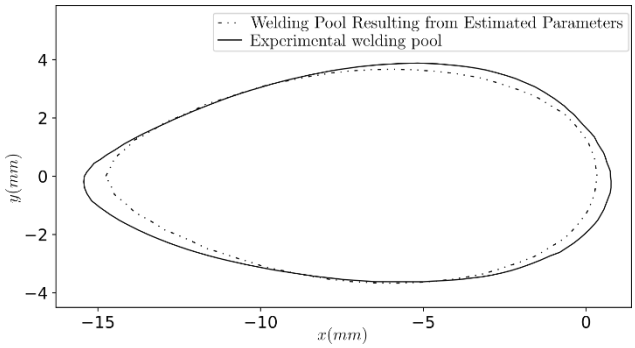

Fig. 6. Weld pool contour comparison between the experimental and numerical ones with estimated parameters.

As shown in figure 6, the weld pool resulting from estimated modelling parameters is in a good agreement with the experimental weld pool.

Concurrently, the estimated unknown parameters, which best fit the experimental data, are leveraged to predict the thermal field. This prediction traditionally involves solving conservation equations using numerical methods like finite element analysis. However, in this study, we exploit the dataset generated for the surrogate model to train a thermal field predictor. The K-Nearest Neighbors (K-NN) regression model is employed for this purpose, predicting temperature values at each node based on the estimated parameters. K-NN prediction involves calculating the distance between a new data point and existing training data points using a chosen distance metric (e.g., Euclidean or Manhattan distance). The predicted temperature value is then determined by averaging the values of its 'K' nearest neighbors. This approach enables the direct reconstruction of the thermal field from the estimated parameters, without requiring the explicit solution of complex equations.

Let's denote our training dataset as $\{\theta_i, T_i\}$, with θ_i the unknown parameters, T_i the corresponding thermal field results from Finite elements calculation. Reconstructing the thermal field results for an unseen data point, derived from the solution of the inverse problem (1), is formulated as follows:

1. Compute the distances between θ_{opt} and all the training samples θ_i given a metric norm. The following formulas introduces some common norms to calculate distances:
   Manhattan distance: $d_{L_1}(p,q) = \sum_{i=1}^{n} \mid q_i - p_i \mid$
   Euclidian distance: $d_{L_2}(p,q) = \sqrt{\sum_{i=1}^{n}(q_i - p_i)^2}$
2. Identify the set of K training samples that are closest to θ_{opt}.
3. The K-NN regressor function would average the corresponding thermal fields of the nearest K neighbors.

There are different ways to calculate the averages in K-NN regression. The most common method involves calculating the average of the output neighbors. The average is expressed as follows:

$$T(\theta_{opt}) = KNN(\theta_{opt}) = \frac{1}{K}\sum_{i=1}^{K} T_i$$

Another method calculates a weighted sum based on the distances between θ_{opt} and the samples training set. This method assigns more weights to the closest neighbors, with the prediction formulated as:

$$T(\theta_{opt}) = KNN(\theta_{opt}) = \frac{\sum_{i=1}^{K} \frac{1}{d(\theta_{opt}, \theta_i)} T_i}{\sum_{i=1}^{K} \frac{1}{d(\theta_{opt}, \theta_i)}}$$

2.4 K-Nearest Neighbors hyperparameters selection

The selection of the number of nearest neighbors, the ranking of these neighbors, and the use of normal or weighted averages are all aspects of hyperparameter tuning. This tuning is performed using a search grid methodology, which involves varying the model's hyperparameters to identify the combination that yields the best performance. Performance is quantified by calculating the dissimilarities between the model-predicted thermal field and the expected thermal field from the validation dataset. Several metrics can be used to measure dissimilarity, including maximum error, explained variance, mean absolute error, and mean squared error.

3 Results and discussion

We present the cross-validation results for different hyperparameters of the K-NN model using Leave-One-Out Cross-Validation (LOOCV), which is particularly useful for small datasets. In LOOCV, each sample is used once as a validation point, with the process repeated until every sample has served as the validation point. The number of iterations equals the number of samples in the dataset. The performance metrics obtained from each iteration are then analyzed and aggregated to evaluate the model's overall performance and robustness under varying hyperparameters. These aggregated results are typically visualized using a box plot, where each box represents the distribution of performance metrics across all LOOCV iterations.

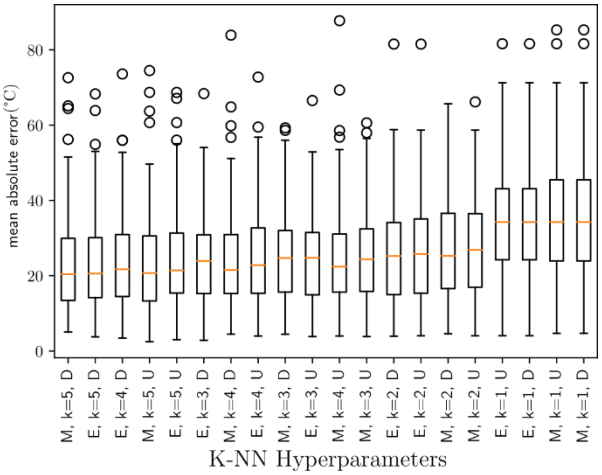

Fig. 7. Ranked Comparison of K-NN Hyperparameters by Mean Absolute Error. (Distance metric: {M: Manhatan, E: Euclidian}, number of neighbors: {k}, sum: {D: Distance (weighted sum), U: Uniform (mean)}.

Figure 7 shows the mean absolute error distribution for the cross-validation results. For thermal field dissimilarity sensing, the mean absolute error metric reflects the average temperature error over all mesh nodes and time steps. Considering this metric, the best-performing K-NN model is achieved with the hyperparameters: Manhattan distance, 5 nearest neighbors, and distance-weighted summation.

Further analysis concerning model hyperparameters selection considering different metric is presented in the following figure 8.

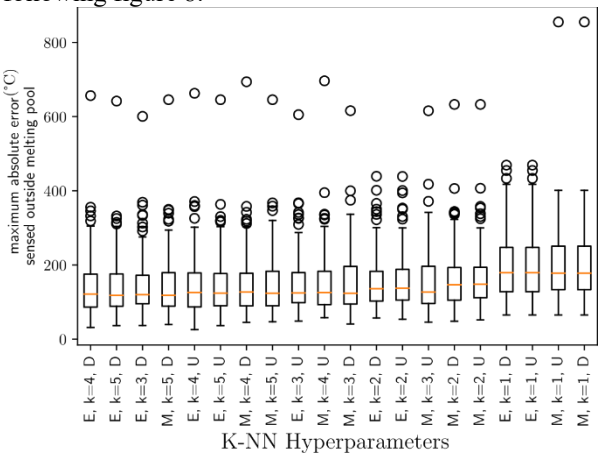

Fig. 8. Ranked Comparison of K-NN Hyperparameters by Maximum Absolute Error Outside Melting Pool Region.

This criterion was chosen because it is still impossible to get the temperature field inside the weld pool experimentally. Furthermore, we aim to use the reconstructed temperature field for thermal-mechanical analysis. Indeed, it is well known that above the melting point, mechanical plastic strains are cancelled out. Given this metric, the ranking of the best K-NN model hyperparameters differs from that based on mean absolute error. The optimal K-NN hyperparameters that minimize this error criterion are listed at the top of the ranking shown in the figure, corresponding to the Euclidean distance metric, 4 nearest neighbors, and distance-weighted summation.

However, mean maximum error over Cross-Validation (CV) iterations does not fully capture the model's performance consistency. A model may perform well in some iterations but poorly in others. The worst performance recorded for the K-NN model over all CV iterations was 656.7 °C, while the best performance recorded was 31.3 °C.

We present the comparison of accuracy and computational time efficiency between the traditional finite element analysis (Figure 9) and the thermal field reconstruction results generated by our K-NN model (Figure 10).

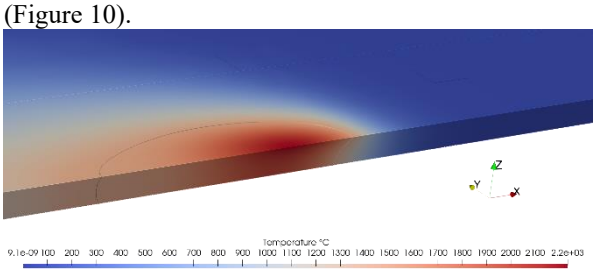

Fig. 9. Thermal field last step resulting from finite elements analysis.

Thermal field reconstruction with K-NN model given the estimated heat source parameters is well represented as shown in figure 10.

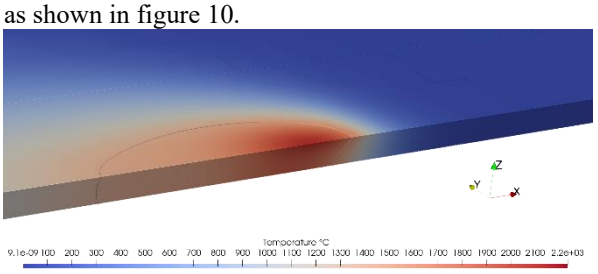

Fig. 10. Predicted thermal field by K-NN regression model.

The computational time required for thermal field prediction using our K-NN regression model was approximately 3.4 seconds. In contrast, traditional finite element analysis took about 12 minutes and 27 seconds, making the K-NN approach approximately 220 times faster.

To assess prediction accuracy, we compared the thermal field results from finite element analysis with those predicted by our K-NN model. Our analysis reveals that the maximum error predominantly occurs within the melt pool region, as shown in Figure 11. Outside this area, the highest error observed locally near the molten region is 201.6°C.

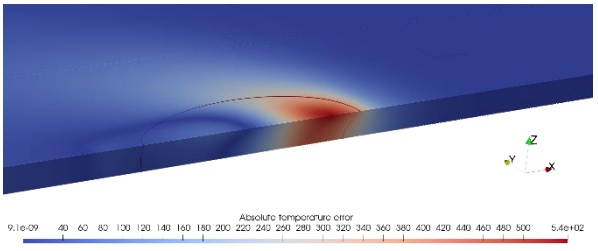

Fig. 11. Absolute difference error between FEM field and K-NN predicted field.

4 Conclusions

This paper introduces a data-driven machine learning approach to predict thermal fields in tungsten inert gas welding applications given a non-intrusive non-destructive camera using surrogate models. Specifically, unknown parameters heat source estimation achieved through optimization framework involving surrogate model, then we applied the K-nearest neighbors (K-NN) regression algorithm and evaluated its performance by varying hyperparameters such as the choice of distance metric, the number of neighbors, and weighting schemes. We compared two metrics, and the results demonstrated that the best model depends on the chosen metric. The optimal K-NN model, identified through our hyperparameter search, showcases satisfactory computational performance, predicting thermal fields 200 times faster than the Finite Element Method. While the thermal field prediction outside the melting pool region is relatively well-represented, meanwhile the maximum absolute error can reach up to 200°C. The effectiveness and consistency of K-NN is limited by the curse of dimensionality, where higher-dimensional input spaces necessitate larger sample sizes to adequately cover parameter variations [9].

Looking ahead, our study reflects on existing methodologies in the literature that have achieved superior thermal field prediction. Notably, model order reduction techniques have been successful in mitigating the curse of dimensionality [10]. Additionally, we suggest enhancing thermal field prediction models by incorporating energy conservation laws. In this context, the selection of the best estimator based on various metrics (e.g., maximum error, explained variance, mean absolute error, mean squared error) significantly impacts the global field prediction accuracy.

To address these challenges, integrating physics conservation laws into predictive modeling—referred to as Physics-Constrained Surrogate Models [11] or physics-informed machine learning [12,13]—offers a rigorous mathematical framework to validate predicted thermal fields. This approach aligns with advancements in the literature aimed at leveraging physics principles to enhance the accuracy and robustness of predictive models for physics-based quantities of interest.

Acknowledgements

This research work was funded by Région Occitanie, France.

References

1. Sindo Kou. Residual Stresses, Distortion, and Fatigue. In: Welding Metallurgy, Chapter 5, 122-141 (2002).
2. Colegrove P., C. Ikeagu, A. Thistlethwaite, S. Williams, T. Nagy, W. Suder, A. Steuwer, and T. Pirling. Welding process impact on residual stress and distortion. Sci. Technol. Weld. Join. **14**, 717–725 (2009).
3. Stephen Cadiou. Modélisation magnéto-thermohydraulique de procédés de fabrication additive arc-fil (WAAM). Theses. Université de Bretagne Sud, Dec. (2019)
4. S. Hilal, Thermo-mechanical modelling of the Wire Arc Additive Manufacturing process (WAAM), Université Paris sciences et lettres, (2022)
5. E. Vaghefi, S. Hosseini, A.H. Afsharinejad, B. Prorok, E. Mirkoohi. Additive manufacturing process parameter design for variable component geometries using reinforcement learning". Addit. Manuf. **84**, 104121 (2024).
6. H. Mu, F. He, L. Yuan, H. Hatamian, P. Commins, Z. Pan. Online distortion simulation using generative machine learning models: A step toward digital twin of metallic additive manufacturing, J. Ind. Inf. Integr. **38**, 100563 (2024).
7. Robert B Gramacy. Surrogates: Gaussian process modeling, design, and optimization for the applied sciences. CRC press, 2020.
8. N. Blanc, I. Bendaoud, C. Bordreuil, F. Deschaux-Beaume, S. Rouquette, F. Soulié, Observations in-situ des mouvements du bain de fusion et des mécanismes de solidification au cours de ligne de fusion TIG, Laboratoire de Mécanique et Génie Civil, (2020).
9. Hastie, Trevor, Robert, Tibshirani and J. H. Friedman, The Elements of Statistical Learning: Data Mining, Inference, and Prediction. New York, Springer, (2009).
10. P. Pereira Alvarez, P. Kerfriden, D. Ryckelynck, V. Robin. Real-Time Data Assimilation in Welding Operations Using Thermal Imaging and Accelerated High-Fidelity Digital Twinning. Mathematics. **9**, 2263 (2021).
11. Y. Zhu, N. Zabaras, P.-S. Koutsourelakis, P. Perdikaris. Physics-constrained deep learning for high-dimensional surrogate modeling and uncertainty quantification without labeled data. J. Comput. Phys. **394**, 56–81 (2019).
12. S. Cai, Z. Wang, S. Wang, P. Perdikaris, G.E. Karniadakis. Physics-Informed Neural Networks for Heat Transfer Problems. ASME. J. Heat Transfer **143**, 060801 (2021).
13. G.E. Karniadakis, I.G. Kevrekidis, L. Lu, P. Perdikaris, S. Wang, L. Yang. Physics-informed machine learning. Nat. Rev. Phys. **3**, 422–440 (2021).